Application of alkali-activated materials (AAM) in seismic and combined energy and seismic retrofitting of beam-type masonry walls

In- and out-of-plane behavior

Azdejkovic, Lazar D.; Triantafillou, Thanasis C.; Papanicolaou, Catherine G.; Miranda de Lima, Luiz

DOI
10.1016/j.engstruct.2025.120207

Publication date
2025

Document Version
Final published version

Published in
Engineering Structures

Citation (APA)
Azdejkovic, L. D., Triantafillou, T. C., Papanicolaou, C. G., & Miranda de Lima, L. (2025). Application of alkali-activated materials (AAM) in seismic and combined energy and seismic retrofitting of beam-type masonry walls: In- and out-of-plane behavior. *Engineering Structures*, *334*, Article 120207. https://doi.org/10.1016/j.engstruct.2025.120207

Engineering Structures 334 (2025) 120207

Contents lists available at ScienceDirect

Engineering Structures

journal homepage: www.elsevier.com/locate/engstruct

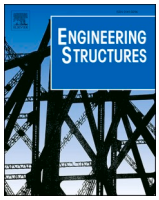

Application of alkali-activated materials (AAM) in seismic and combined energy and seismic retrofitting of beam-type masonry walls: In- and out-of-plane behavior

Lazar D. Azdejkovic [a,*], Thanasis C. Triantafillou [a], Catherine G. Papanicolaou [a], Luiz Miranda de Lima [b]

[a] University of Patras, Department of Civil Engineering, Structural Materials Lab, Patras 26500, Greece
[b] Delft University of Technology, Department of Materials and Environment (Microlab), Faculty of Civil Engineering and Geosciences, Stevinweg 1, Delft 2628 CN, the Netherlands

ARTICLE INFO

Keywords:
Alkali-activated materials
Cyclic loading
Durability of glass-fiber textile
Energy retrofitting
Geopolymers
Masonry walls
Seismic retrofitting
Textile reinforced mortar

ABSTRACT

The application of alkali-activated materials (AAM) based on metakaolin, fly ash and ladle furnace slag in seismic retrofitting of beam-type unreinforced masonry (URM) walls with textile reinforced mortars (TRM) was investigated in this study. Additionally, a combined seismic and energy retrofitting scheme comprising an extruded polystyrene (XPS) thermal insulation, alkali-activated or traditional cementitious mortar and styrene-butadiene rubber (SBR)-coated glass-fiber textile was studied on beam-type URM walls. A total of 12 wall specimens made of perforated fired-clay bricks were subjected to in- and out-of-plane cyclic tests. Seismic retrofitting with AAM-based TRM led to a substantial increase of load-bearing capacity, up to 70 %, while the combined energy and seismic retrofitting increased the energy dissipation capacity by at least 8 times for both in- and out-of-plane loading. Durability of the TRM jackets consisted of SBR-coated glass-fiber textile and AAM mortar was studied experimentally and at the matrix-fiber interface with Scanning Electron Microscopy (SEM) and Energy Dispersive X-ray Spectroscopy (EDS). A severe impact of the AAM mortar mix in fresh state on SBR-coated glass-fiber textile was quantified through a set of uniaxial tensile tests and confirmed at a microscopic level. Alkali-activated materials pose a great potential in becoming an effective and environmentally friendly alternative to traditional cementitious materials in structural repair and retrofitting applications. However, to systematically utilize the AAM-based TRM strengthening configurations studied here, the addressed durability issues need to be resolved.

1. Introduction

Despite the wide use of versatile, modern building materials (reinforced concrete, steel), unreinforced masonry (URM) still remains the most prevailing building material in the existing building stock, worldwide. Most of the URM structures were constructed before the introduction of strict building codes, with some of them representing cultural heritage buildings, while the vast majority is still in everyday use (residential or commercial). More than 80 % of the buildings in Europe are at least 30 years old, while 40 % were constructed before the 60's [1]. Therefore, a number of techniques have been developed over the years in order to upgrade the existing buildings to meet the current standards and demands. Grout injection, mortar jacketing (plastering), addition of steel reinforcement, external jacketing with steel or fiber reinforced polymers (FRP) are some of the most common seismic retrofitting strategies applied at URM buildings. Researchers have proposed an alternative solution to seismic retrofitting with FRP, namely textile reinforced mortars (TRM), in which inorganic binders are combined with fiber-yarn textiles [2,3]. TRM is considered to be a more appropriate retrofitting technique for masonry structures compared to FRP, for several reasons: compatibility with the masonry substrate, better behavior at high temperatures, easier application, etc. [4]. These materials can also be found in the literature under different names, such as textile-reinforced concrete (TRC) or fabric-reinforced cementitious

* Corresponding author.
E-mail addresses: lazar@upatras.gr (L.D. Azdejkovic), ttriant@upatras.gr (T.C. Triantafillou), kpapanic@upatras.gr (C.G. Papanicolaou), L.MirandadeLima@tudelft.nl (L. Miranda de Lima).

https://doi.org/10.1016/j.engstruct.2025.120207
Received 23 December 2024; Received in revised form 10 March 2025; Accepted 25 March 2025
Available online 9 April 2025

matrix (FRCM).

The applicability of TRM strengthening jackets on shear and beam-like URM walls made of fired-clay bricks was studied by Papanicolaou et al. [4,5], where the wall specimens were subjected to in- and out-of-plane cyclic three-point bending tests. Seismic retrofitting with TRM of URM pier-spandrel sub-assemblages made of different brick materials (tuff, stone, fired clay) was investigated as well [6–8]. In the study by Augenti et al. [6], the effectiveness of TRM jackets applied on shear-deficient URM spandrel walls was confirmed with in-plane cyclic tests. The effectiveness of the TRM strengthening system was studied experimentally through large scale tests of U-shaped URM structure [9]. The experimental outcomes in which the TRM jackets decreased the damage induced by pseudo-dynamic loading with a significant increase of load bearing and displacement capacity of the URM structure were confirmed numerically [10]. A significant improvement in the out-of-plane response of the URM walls retrofitted with TRM was reported in the published research studies [7,11,12]. The potential utilization of TRM in the form of confining jackets applied on square and rectangular URM columns made of fired clay bricks was studied in [13,14].

Due to the general tendency of European society to reach carbon neutrality by 2050 [15], the process of reshaping the industry with novel technologies, production optimizations and sustainable energy sources has already started. Thus, alternative cementitious materials that could reduce or potentially replace ordinary Portland cement - the production of which is responsible for more than 6 % of the global CO_2 emissions - became interesting for the research community, worldwide. Therefore, strengthening schemes based on alternative binders such as natural lime or geopolymers reinforced with textiles were studied from the fiber-matrix interface up to the large-scale applications [16–20]. Natural lime as a building material has shown great potential in reducing the environmental impact of the TRM strengthening system by maintaining the respectable level of performance when applied on URM masonry walls subjected to in- and out-of-plane loading [21–23].

Despite the different binder nomenclature, geopolymers [24] are considered hereafter as a subdivision of alkali-activated materials (AAM) [25] and thus, these two terms are treated as synonyms. Even though the AAM technology has found its application in the construction industry in the former USSR [26], numerous potential applications are still being studied, including the repair and seismic retrofitting of existing structural elements. As mentioned earlier, the concept of the textile reinforced geopolymers was studied by various researchers worldwide e.g. [27–30], just a few research studies covered the seismic retrofitting of existing structures with textile reinforced alkali-activated mortars (TRAAM). In [21] a geopolymer mortar was combined with basalt-fiber textile to strengthen URM walls made of natural stone walls. The performance of AAM-based and cementitious TRM strengthening schemes was compared in a study by [31] through cyclic tests of shear-deficient RC columns, while the potential applications of TRAAM jackets on masonry infills of RC frames were investigated through a set of diagonal compression tests in [18,32,33].

The existing building stock in Europe requires systematic renovation with the aim of improving energy performance and reducing the environmental impact. This catalyzed the development of new solutions for combined structural and energy upgrading [34–36]. To tackle the need for seismic and energy retrofitting of existing buildings in southern Europe, a promising integrated technique consisting of TRM overlays externally bonded with thermal insulation plates was proposed by Triantafillou et al. [37,38]. This system has excellent potential to perform well at a cost significantly lower compared to the independent execution of the two interventions [39]. The efficacy of the integrated seismic and energy upgrade based on TRM coatings and expanded polystyrene (EPS) thermal insulating panels was proved on beam-type URM wall specimens made of perforated fired-clay bricks that were subjected to cyclic or monotonic in- and out-of-plane loading [35,36,40,41]. Moreover, in a study by Gkournelos and Triantafillou [42] the integrated retrofitting

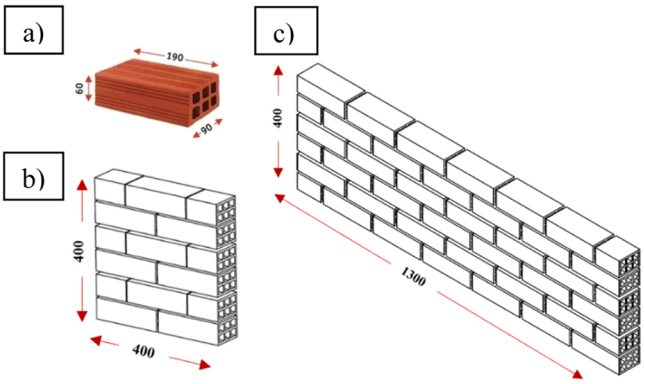

Fig. 1. Schematic representation of perforated fired-clay brick masonry walls: a) perforated clay brick; b) compression test specimen; c) beam-type wall specimen.

was applied at pre-damaged RC frame masonry infills, and subjected at first to cyclic in-plane, and consecutively to monotonic out-of-plane loading.

A tremendous need for a sustainable alternative to traditional cementitious binders, caused by the general tendency of lowering greenhouse gas emissions was decisive for studying the application of AAM mortar as the TRM strengthening system matrix material. Moreover, a preliminary investigation of combined seismic and energy retrofitting was carried out aiming to further reduce the environmental impact of the system proposed in [34,37] with the utilization of geopolymer (AAM) mortar. A great majority of the authors that analyzed the life cycle assessment of AAMs in general agree that these materials have lower global worming potential compared to OPC [43–45].

The presented paper studies experimentally the strengthening of beam-type masonry walls made of perforated fired-clay bricks through a set of in- and out-of-plane cyclic four-point tests. Shear-critical beam-type URM walls strengthened with two different TRAAM retrofitting schemes (seismic, and combined energy and seismic) were subjected to cyclic in-plane loading, which to the authors' best knowledge has not been studied so far. For comparison, a scheme comprising an ordinary Portland cement (OPC)-based TRM and thermal insulation was tested, too. Apart from the URM wall specimens tested in-plane, the same group of specimens was subjected to cyclic four-point bending tests with the loading imposed out-of-plane. Although the numerical and analytical modeling of URM walls retrofitted with TRM represents an interesting research field so far successfully covered in several publications [46–48], this topic is beyond the scope of this paper.

Durability of TRAAM composites can potentially represent a hurdle in the process of adoption and wider use of these materials by the community. Therefore, different combinations of AAMs and textiles (e.g. glass, basalt, carbon, jute) have been studied extensively by researchers worldwide focusing on durability of TRAAM [10,49–52]. This paper investigates the potential durability issues of the proposed AAM-based TRM composite through a set of tensile tests and by performing scanning electron microscopy (SEM) and energy-dispersive spectroscopy (EDS) at the fiber-matrix interface.

2. Materials, methods and experimental program

2.1. Materials and specimens

2.1.1. Clay brick masonry wall specimens

A total of 12 single-leaf beam-type wall specimens were built with dimensions 1300 × 400 × 90 mm. A general-purpose masonry mortar was produced on site using cement, lime putty, sand, and water, in a ratio of 1:1:5:0.75 by volume (or 1:0.5:3.6:0.27, by weight), and it was combined with hollow clay bricks to construct beam-type wall

Table 1
Overview of the alkali-activated mortar mix (quantities are expressed in grams per 1 kg of precursors).

MK	LFS	FA	K_2SiO_3	KOH	H_2O	Sand	PVA fibers[a]
523.8	152.4	323.8	533.3	95.2	304.8	1695	0.25 %

(MK – metakaolin; LFS – ladle furnace slag; FA – fly ash)
[a] per fresh mortar volume.

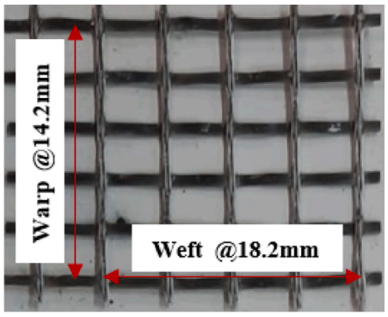

Fig. 2. SBR-coated glass-fiber textile used in the TRM strengthening system.

specimens (Fig. 1). Standard perforated fired-clay bricks with six perforations running lengthwise were laid flat on their largest side so that perforations were oriented parallel to the mortar bed joints (Fig. 1); thus, the wall thickness was defined by an individual brick width. Such a geometry was decided upon to simulate parapets, spandrels and the upper segments of URM walls, especially when subjected to out-of-plane seismic action. Two identical groups of six wall specimens were constructed for in- and out-of-plane cyclic testing (Fig. 1c). Two masonry wallettes (400 × 400 × 90 mm) were built as well and subjected to monotonic uniaxial compressive loading to characterize the constructed masonry and the construction quality (Fig. 1b).

2.1.2. Retrofitting with AAM-based TRM jackets

A total of four specimens were strengthened with AAM-based TRM jackets without applying thermal insulation, out of which two were subjected to in-plane and the other two to out-of-plane cyclic loading. An alkali-activated mortar mix design developed and tested in [53] was utilized as TRM matrix material in this study. The AAM mix consisting of metakaolin, fly ash and ladle furnace slag, was activated with potassium-based activators' solution (Table 1). Short (6 mm) polyvinyl-alcohol (PVA) fibers were included into the AAM mortar mix, which was combined with a commercial alkali-resistant (AR) styrene-butadiene rubber (SBR)-coated E-glass fiber textile to form a TRM strengthening product. The net weight of the textile in the two directions was 145 g/m^2 and 135 g/m^2, respectively (Fig. 2), while the total unit weight with coating was 360 g/m^2. Since the fiber density of the textile grid is 2600 g/m^3, the equivalent nominal thickness (based on smeared distribution of the fibers) would be equal to 0.056 mm in the warp direction, and 0.052 mm in the weft direction.

The chemical solution used for activation of the alkali-activated (geopolymer) mortar mix was prepared at least one day prior to the mortar application. The short PVA fibers were added to the dry mix of precursor powders for obtaining an adequate distribution among the matrix before the addition of the activating solution. The mixing of dry powders with activators was realized with an electric hand mixer until a homogeneous paste was formed. Finally, the aggregates were added to the formed paste and the mixing continued for at least three minutes. After the mixing was completed, the fresh mortar was left in a bucket to settle for at least 5 min until being applied.

The primary mortar layer was applied on a well wetted wall surface, in approximately 3–5 mm thick layers after which the first layer of textile was applied and pressed with a metal trowel into the applied mortar, keeping the fiber rovings in both directions straight and assuring that the mortar protrudes through the textile grid openings (Fig. 3a). The next mortar layer, approximately 2 mm thick, was applied so that it fully covered all fiber yarns of the previously applied textile layer. This procedure was either repeated on the opposite side of the wall or another layer of the textile grid was added by repeating the "wet lay-up" procedure (Fig. 4). The TRM-strengthened walls were cured under wet burlaps for three days to prevent the drying shrinkage caused by the rapid moisture loss. The walls were then kept inside the lab under ambient conditions at approximately 20ºC and a relative humidity of 50 % for approximately one month before testing.

2.1.3. Combined seismic and energy retrofitting

Integrated seismic and energy retrofitting was applied on one side of the beam-type walls made of hollow clay bricks in a TRM/insulation/TRM stratified configuration. Two TRM systems were applied, both using a single-layer of the same glass-fiber textile (Fig. 2) which was embedded either in the alkali-activated mortar (Table 1) forming TRAAM, or in a commercial polymer-modified OPC-based product specially developed for gluing insulating materials, forming a textile reinforced cementitious mortar (TRCM). The insulating extruded polystyrene board (30 mm in thickness) was sandwiched between the two TRM layers (Fig. 4). The specimens were retrofitted with the two outer product layers (insulation/TRM) covering the entire width of the specimens while extending (lengthwise) between the support lines. The four circular cutouts (Ø70 mm) were made on each of the XPS panels (two for each load application line) and applied on the specimens to be subjected to out-of-plane tests. When the inner TRM layer and the insulation board were in place these holes were filled with mortar (AAM or OPC – depending on the case), so that the loading was not imposed directly over the XPS boards (Fig. 3b); thus, unwanted anchorage of the panels along the loading lines was avoided. Preparation of a polymer-modified commercial OPC-based mortar was carried out simply by adding water to the ready-made dry mortar mix according to the manufacturer's instructions (using a water-to-solid weight ratio of 0.2). Mixing was done

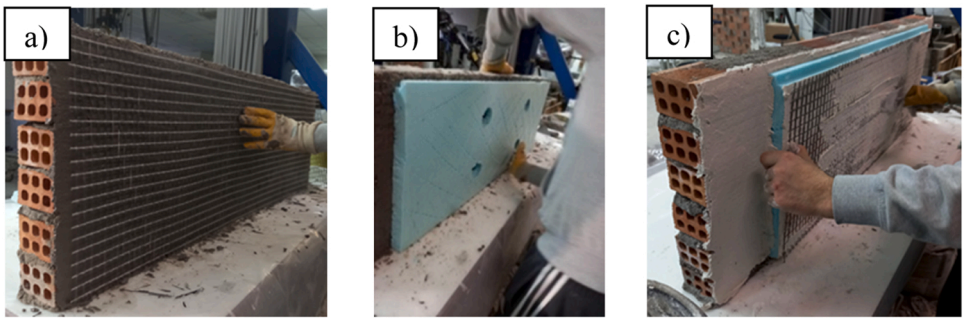

Fig. 3. Seismic and combined retrofitting of beam-type walls: a) First TRAAM layer application; b) XPS application on top of the TRAAM layer; c) Second textile reinforced cementitious mortar (TRCM) layer application.

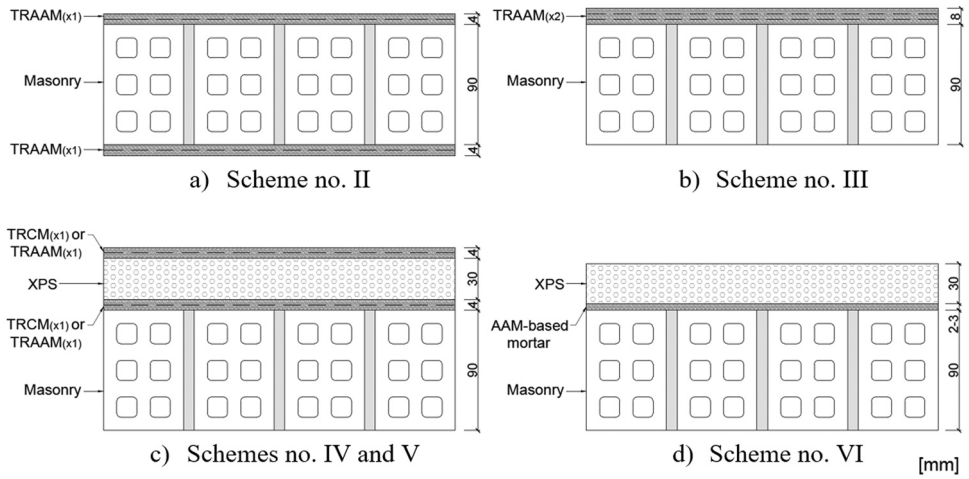

Fig. 4. Schematic detailing of the retrofitted wall configurations and their numeration: a) double-sided seismic retrofitting (no. II); b) single-sided seismic retrofitting (no. III); c) combined seismic and energy retrofitting with AAM-based or OPC-based TRM and XPS (no. IV, V); d) energy retrofitting with XPS and AAM-mortar (no. VI).

with an electric hand-held mixer for approximately five minutes, after which the application to wetted wall surface took place.

The combined seismic and energy retrofitting system was applied by following the "wet lay-up" procedure. After applying the inner single-layered TRM jacket (AAM- or OPC-based), the thermal-insulating XPS board was bonded onto the external mortar layer of the TRM (Fig. 3b). Then, the board was fully covered by a thin mortar layer (2–3 mm, AAM or OPC – depending on the case) and the external TRM jacket was applied (Figs. 3c, 4).

Because the axial stiffness (elastic modulus = 20 MPa, thickness = 30 mm) of the applied XPS boards is not negligible, two specimens (one for in-plane and another for out-of-plane loading) were retrofitted by only bonding one XPS board directly onto the wall surface by means of the AAM mortar (Fig. 4). In this way, the influence of the XPS thermal insulation combined with the AAM mortar (Table 1) on the deformation capacity and the cracking distribution of the beam-type walls was also studied.

The applied commercial OPC-based mortar was designed for in-situ application of thermal insulating boards on masonry walls. Thus, its workability, adhesion to substrate materials, and mechanical characteristics are optimized for a wide range of conditions and possible applications. On the other hand, the AAM mortar mix was developed as low carbon footprint alternative for commercial high-performance repair mortars [53]. Due to the high concentration of potassium-based activators, the TRAAM system had some major disadvantages regarding the ease-of-application: the preparation procedure, workability, and the causticity of the mortar in fresh state which can be hazardous when in contact with skin. Therefore, applying the TRAAM system to the walls in-situ was much more challenging than the TRCM one.

A simple cost comparison was carried out between the two strengthening systems reinforced with a single layer of the SBR-coated glass-fiber textile (TRAAM and TRCM), and a *control* one currently popular in the Greek market consisting a commercial cement-based repair mortar and a single layer of the same textile material. The cost analysis based on the available market data showed that the cost of the applied TRAAM system is 16 % higher than the *control* and 44 % higher than the TRCM one, primarily due to the high costs of the activating chemicals. Further optimization of the AAM mix design could lower the price considerably. In any case, it is noted that the pricing ratios are limited to this experimental campaign and may differ significantly in other markets.

Table 2
Overview of the TRM material characterization testing outcomes.

Material	Property	Number of specimens	Average values of the mechanical capacity (standard deviation in parentheses)
Alkali-activated mortar	f_t [MPa][a]	3	5.8 (0.1)
	f_c [MPa][b]	6	42.4 (2.2)
Polymer-modified OPC mortar	f_t [MPa]	3	4.2 (0.4)
	f_c [MPa]	6	11.7 (0.2)
SBR-coated bare glass-fiber textile	F_t [kN/m][c]	3	61.6 (0.5)
	f_t [MPa][d]		1184.3 (9.7)
	ε_{tu} [%][e]		2.349 (0.162)
Double-layered TRAAM	F_t [kN/m][c]	4	19.8 (1.7)
	f_t [MPa][d]		381.0 (33.6)
	ε_{tu} [%][e]		0.663 (0.196)
Double-layered TRCM	F_t [kN/m]	4	34.2 (1.2)
	f_t [MPa]		658.2 (22.6)
	ε_{tu} [%]		2.323 (0.235)

[a] Flexural strength of mortar;
[b] Compressive strength of mortar;
[c] Tensile strength per unit width of a single textile layer;
[d] Tensile strength referring to the fibers' cross-section;
[e] Tensile strain at fiber-roving rupture.

2.2. Material characterization

A set of standard flexural and compressive tests were carried out on prismatic mortar specimens cured for 28 days, according to EN196-1 [54]. The mortars were cast into standard steel moulds, which were covered with a polyethylene foil for one day, in order to prevent the rapid loss of moisture. Around 24 h after casting, the mortar prisms were demoulded, and were kept for the next two days under wet burlaps, after which were left on a shelf in the lab (approximately 20 °C, RH 50 %) until the day of testing. An overview of mortar testing outcomes is included in Table 2.

Tensile coupon specimens comprising two glass-fiber textile reinforcement layers embedded in either a polymer-modified cementitious mortar (TRCM – textile reinforced cement-based mortar) or in an alkali-activated mortar (TRAAM – textile reinforced alkali-activated mortar) were subjected to uniaxial tension tests according to AC434 [55]. Production of double-layered TRM coupons was realized in metallic moulds

Table 3
Overview of the masonry and mortar characterization test results.

Material	Property	Number of specimens	Average values of the mechanical capacity (standard deviation in parentheses)
Hollow clay bricks	$f_{c,\perp}$ [MPa][a]	3	9.8 (3.0)
	$f_{c,\parallel}$ [MPa][b]	3	25.8 (1.0)
Masonry mortar	f_t [MPa][c]	3	1.9 (0.1)
	f_c [MPa][d]	6	7.2 (0.4)
Masonry wallettes	f_c [MPa]	2	5.4 (2.6)

[a] Brick compressive strength in direction perpendicular to the holes;
[b] Brick compressive strength in direction parallel to the holes;
[c] Flexural strength of mortar;
[d] Compressive strength.

with dimensions 95 × 700 mm, by following the same procedure applied in retrofitting of walls. The freshly cast specimens were kept under PE foil for one day until they were demoulded. The curing continued for two more days under wet burlaps. The cast TRM coupons (TRCM and TRAAM) were kept under ambient lab conditions (20 °C, RH 50 %) until the age of 28 days. Steel tabs were bilaterally glued to both ends of each specimen with epoxy resin. Clevis-type connectors and hooks allowing for rotation both in and out of the coupons' plane were used to connect the TRM specimens to the testing machine. Tensile testing of the bare glass-fiber textile was carried out according to ISO 13934-1 [56]. Five rovings wide and 650 mm long SBR-coated bare glass-fiber textile specimens bearing end-tabs (same as above) were hydraulically clamped by the grips of the testing machine. A servo-hydraulic testing machine with a capacity of 250 kN was used for all tensile tests, which were carried out in displacement control at a loading rate of 0.003 mm/s. Real-time deformation measurements were acquired with a video-extensometer apparatus, while the loads were obtained directly from the loadcell controller.

The results of all tensile tests are listed in Table 2, including: the tensile strength, defined as maximum attained load divided by longitudinal (load-aligned) fiber area (in the case of bare textile, also expressed as maximum attained load per unit textile width), and ultimate tensile strain. The TRAAM specimens exhibited a lower strength and deformation capacity compared to the bare glass-fiber textile specimens by 68 % and 72 %, respectively. The TRCM coupons performed significantly better than their TRAAM counterparts, with a lower tensile strength and deformation capacity by 44 % and 1.1 %, respectively, compared to the bare glass-fiber textile specimens (Table 2). Despite the large difference in responses, both tested TRM systems can be qualified as strain-hardening inorganic composites.

The compressive strength of the clay bricks in directions parallel and perpendicular to the perforations was derived from three uniaxial compression tests. The bearing surfaces of the individual brick specimens were capped using a self-leveling, rapid-hardening mortar. Building mortar prisms, cast during the construction of beam-type URM walls, were subjected to standard compressive and flexural tests (EN196–1) [54]. The results of these tests are included in Table 3. Mean compressive strength of the square masonry wallettes in the direction perpendicular to the bed joints was obtained through compression tests conducted on two specimens (Fig. 1c). These wallettes were constructed and tested at the same time as the main beam-type wall specimens, at an age of approximately two months. The surfaces of the wallettes that were in contact with the compression platens were capped using a normal-strength cement mortar to achieve a better load transfer. The compression tests were carried out in displacement control mode at a constant loading rate equal to 0.01 mm/s, using a 4000 kN loading-capacity testing machine. Loads were obtained directly from the load cell, while displacements were measured continuously using a video-extensometer apparatus.

2.3. Experimental procedure and setup

An overview of the specimens subjected to in- and out-of-plane cyclic loading with their retrofitting configurations and the numerations which correspond to the schemes given in Fig. 4 is given in Table 4. Each specimen is assigned an ID which follows the order of applied layers. For instance, "W_TRAAM$_{x1}$_XPS_TRAAM$_{x1}$" denotes the wall retrofitted with combined seismic and energy system with two single-layered AAM-based TRM jackets, where "W" stands for wall, "TRAAM$_{x1}$" or "TRCM$_{x1}$" denote the applied strengthening jacket with number of layers in index (textile reinforced alkali-activated mortar or textile reinforced cement-based mortar, respectively), while "XPS" stands for the applied thermal insulation. In case of the specimens furnished only with XPS boards which were bonded with alkali-activated mortar, the "W_XPS" specimen ID applies. Two specimens of each ID with identical configurations were prepared, one for in-plane and the other for out-of-plane cyclic testing.

The experimental program consisted of cyclic in- and out-of-plane tests, performed in a strong frame, using a four-point bending testing configuration (Fig. 5). This configuration primarily aims to simulate the out-of-plane response typically observed in URM spandrels, parapet walls, and upper wall segments of buildings without rigid diaphragms as slabs. In case of the in-plane tests, the same four-point bending setup was used to evaluate the relative effectiveness of the seismic (TRAAM) and combined seismic and energy upgrade (TRAAM or TRCM and XPS) when applied at URM beam-type walls with horizontally oriented mortar bed joints. The specimens' geometry and in-plane test setup limit the scalability of the observed results to full-scale structures, except in case of specific type of deep beam-type of walls which sustain a diagonal shear failure mechanism (e.g. weak spandrels or spandrels supported by flexible lintel beams [57]).

The displacement time history was imposed by a vertically positioned servo-hydraulic actuator, operated in a displacement control regime with a rigid steel spreader beam fixed to the actuator's head (Fig. 5). The load was transferred at the two points/lines positioned 400 mm from the end-supports (Fig. 5) over a set of metallic hinges. Four steel hollow sections and a pair of metallic hinges placed beneath the specimen were connected to the actuator with four prestressed steel threaded rods enabling negative (upward) loading. A set of metallic hinges, sections and steel rods ensured rotational freedom at the supports and made possible the application of negative (upwards) piston displacements by providing support to the negative loading in both in-

Table 4
Test matrix with the retrofitting parameters.

No.	Single-/double-sided retrofitting	Type of mortar used for retrofitting	Number of TRM layers (side1/side2)	Energy retrofitting	Specimen ID
I	-	-	-	-	Control
II	Double-sided	AAM-based	1/1	-	TRAAM$_{x1}$_W_TRAAM$_{x1}$
III	Single-sided	AAM-based	0/2	-	W_TRAAM$_{x2}$
IV	Single-sided	AAM-based	0/2	XPS	W_TRAAM$_{x1}$_XPS_ TRAAM$_{x1}$
V	Single-sided	OPC-based	0/2	XPS	W_TRCM$_{x1}$_XPS_ TRCM$_{x1}$
VI	Single-sided	AAM-based	-	XPS	W_XPS

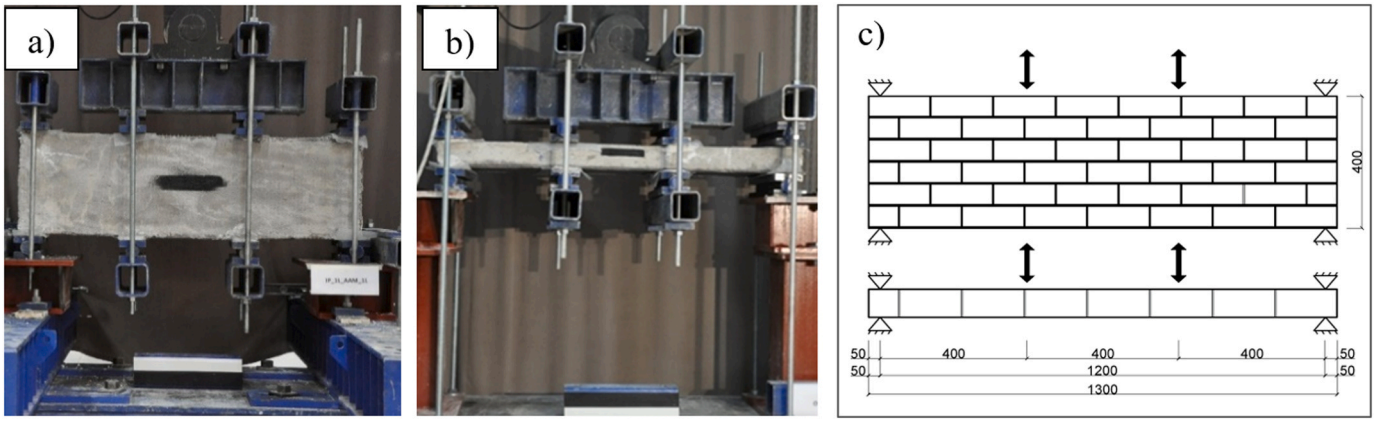

Fig. 5. Photo representation of: a) In-plane testing setup; b) Out-of-plane testing setup; c) Schematic representations of the two setups (mm).

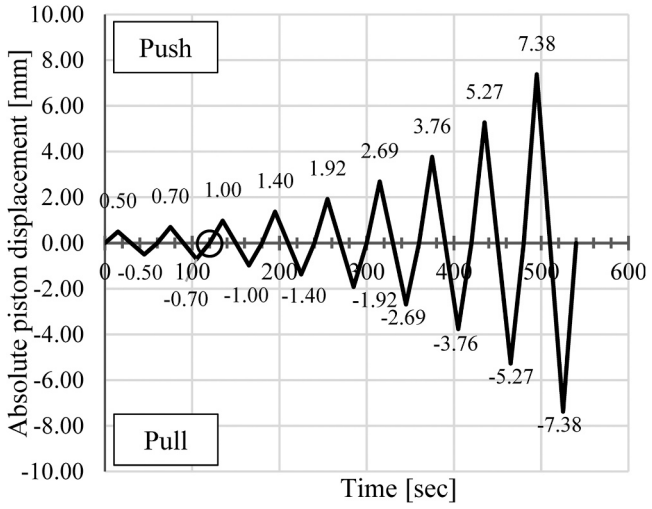

Fig. 6. Displacement time history applied in testing of clay-brick masonry walls.

and out-of-plane configurations.

Displacements were measured at the mid-span of each specimen with a video-extensometer apparatus, while the load measurements were acquired directly from the actuator's loadcell. A camera was placed 3 m in front of the specimen and connected to the computer, which via dedicated software tracked in real-time the distance between two specified points; one was placed on the element at the point of interest (black marks at the middle of the specimens, Fig. 5a, b) and another at a fixed place on the strong frame. That way, the displacements were accurately monitored externally without being affected by local failures or cracks that would occur during the experiments.

The displacement time-history (Fig. 6) was imposed by the vertically positioned servo-hydraulic actuator in all tests. Regarding in-plane tests, the targeted displacement of the initial cycle was 0.5 mm, while in every following cycle the targeted displacements were increased by an increment factor of 1.4, as recommended in FEMA461 [58]. Due to the significantly lower out-of-plane stiffness, the initial two cycles shown in Fig. 6 were neglected in the out-of-plane tests; thus, the initial cycle of the displacement time-history was 1 mm. The increment factor applied in the following cycles was the same as that for the in-plane tests (1.4). Therefore, the out-of-plane loading cycles were identical to those presented in Fig. 6 from the 3rd cycle onwards, and the starting point of the applied displacement time history is marked in Fig. 6 with a circle.

3. Experimental results and discussion

An overview of the test results is presented in Table 5, including peak load values, displacements at failure in push and pull direction (at the abrupt load drop), dissipated energy prior to the failure occurrence at both sides of the specimen (complete cross-section failure) and observed failure mode after which the specimen lost its load-bearing capacity in

Table 5
Overview of the cyclic testing results.

Specimen ID	Peak Load [kN]		Peak displacement prior to failure [mm] [a,b]		Cycle of complete failure	Dissipated energy [Nm]	Failure mode
	Push	Pull	Push	Pull			
In-plane							
Control	17.4	18.3	0.53	−0.22	3	26.1	Diagonal shear
$TRAAM_{x1}$_W_$TRAAM_{x1}$	33.7	27.6	0.87	−0.88	4	78.2	Textile rupture (push)
W_$TRAAM_{x2}$	29.4	26.5	2.62	−2.27	6	380.1	Textile rupture (push)
W_$TRAAM_{x1}$_XPS_ $TRAAM_{x1}$	27.5	28.6	2.45	−0.54	6	290.5	Textile rupture (push)
W_$TRCM_{x1}$_XPS_ $TRCM_{x1}$	29.6	24.6	2.60	−0.36	6	213.8	XPS debonding/textile rupture (push)
W_XPS	24.2	23.1	0.79	−0.39	3	48.8	Flexure
Out-of-plane							
Control	9.6	9.8	1.98	−0.65	4	37.7	Flexure
$TRAAM_{x1}$_W_$TRAAM_{x1}$	10.9	11.7	3.35	−2.94	6	153.8	Textile rupture (push)
W_$TRAAM_{x2}$	17.3	9.7	3.86	−0.85	6	135.4	Textile rupture (push)
W_$TRAAM_{x1}$_XPS_ $TRAAM_{x1}$	15.2	9.3	5.0	−1.41	7	180.8	Textile rupture (push)/ XPS debonding
W_$TRCM_{x1}$_XPS_ $TRCM_{x1}$	13.7	9.5	11.60	−7.25	8	445.8	XPS debonding (push)/ brick failure
W_XPS	n/a		n/a		4	n/a	Flexure

[a] Corresponding to sudden load reduction or to 80 % of the peak load (post-peak branch) in case of gradual post-peak reduction;
[b] Midspan displacement for in- and out-of-plane tests at partial (on a single side) or full section failure.

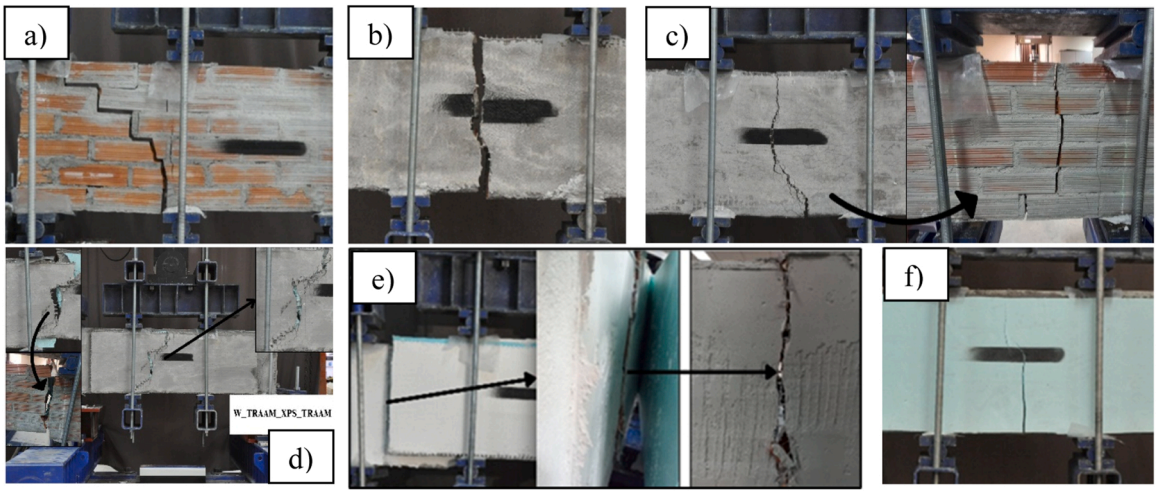

Fig. 7. In-plane test failures: *diagonal shear* - a) Control; *textile rupture* - b) $TRAAM_{x1}$_W_TRAAM_{x1}, c) W_TRAAM_{x2}, d) W_TRAAM_{x1}_XPS_TRAAM_{x1}, *XPS debonding/ textile rupture* - e) W_TRCM_{x1}_XPS_TRCM_{x1}; *flexure* - f) W_XPS.

both directions. The out-of-plane test of the specimen W_XPS was unsuccessful and therefore the results are not shown. Hysteretic loop diagrams in which the response of the tested specimens is presented as a function of the total vertical load and the respective midspan displacement are presented in Fig. 8 for in-plane tests, and in Fig. 11 for out-of-plane tests, with the points of complete failure marked with circle markers. Envelopes of the recorded response diagrams and cumulative energy dissipation diagrams as a function of the loading cycle sustained by each specimen are shown for in- and out-of-plane tests in Figs. 9 and 12, respectively. Stiffness degradation of the beam-type wall specimens during the in-plane cyclic tests is presented in a form of the secant stiffness of each cycle, including the one when a complete failure occurred.

3.1. *In-plane four-point bending tests*

The response of the unretrofitted control specimen subjected to in-plane loading can be described as brittle with a typical shear-governed failure. The first crack and a major stiffness reduction occurred during the first cycle in the pull direction, while the complete failure occurred during the third cycle in the downward (push) direction at the (left) shear span following a diagonal shear failure mechanism (Fig. 7a). The application of a single layer of TRAAM on each side of the wall resulted in an average load capacity increase of 72 % (in both directions). The wall retrofitted with two TRAAM layers placed on one side of the wall (W_TRAAM_{x2}) failed completely during the sixth cycle, with an average strength in both directions being 57 % higher than that of the unretrofitted (control) specimen. Failure of both W_TRAAM_{x2} and $TRAAM_{x1}$_W_TRAAM_{x1} specimens was caused by the fibers' rupture near the mid-span (Fig. 7b, c), which in case of the latter occurred at low midspan displacements, indicating a potential reduction of the textile reinforcement deformation capacity. W_TRAAM_{x2} outperformed other specimens subjected to in-plane loading in terms of the energy dissipation and deformation capacity, with the recorded increase of 1350 % and 660 %, respectively (Fig. 9a, b). In case of the double-sided TRAAM application of ($TRAAM_{x1}$_W_TRAAM_{x1}) this increase was only 200 % and 180 %, respectively (Fig. 9a, b).

In-plane tests on specimens retrofitted with combined seismic and energy configurations have shown that the outer TRM layers were not fully activated. The limited transfer of stresses to the outer TRM layer was caused mainly due to the lower stiffness and the limited bond strength of the XPS panels. Specimen W_TRAAM_{x1}_XPS_TRAAM_{x1} developed the first major crack at mid-span in the vicinity of the line of loading. The fiber-rovings of the inner TRM layer active in the push direction started to rupture during the second cycle until complete failure was reached in the sixth cycle when the outer TRM layer and the XPS panel fully failed as well (Fig. 7d). Thus, the peak load reached similar values in the push and pull direction, but the overall response was highly non-symmetric (Fig. 8d), due to the successive rupturing of fiber-rovings along the wall height, which occurred prematurely. Asymmetric in-plane response of W_TRCM_{x1}_XPS_TRCM_{x1} specimen was observed as well, with the initial crack opening during the first cycle (pull direction) in the zone of maximum shear and bending moment. The contribution of the outer TRCM layer was lost during the second cycle when the local debonding of the XPS board took place. Failure of this specimen was governed by glass-fiber rupture of the solely active, inner TRCM layer (Fig. 7e), which occurred at a peak displacement three times higher compared to the corresponding specimen with a single active TRAAM layer at each side ($TRAAM_{x1}$_W_TRAAM_{x1}). Despite a clear premature rupture of SBR-coated glass-fiber rovings exposed to AAM, the total dissipated energy during the in-plane test of W_TRAAM_{x1}_XPS_TRAAM_{x1} wall was 35 % higher than that of its TRCM counterpart, which lost a significant portion of its capacity due to early debonding of the XPS panel. However, secant stiffness of W_TRAAM_{x1}_XPS_TRAAM_{x1} specimen rapidly decreased, from initially 70 % higher value to 26 % lower than that of W_TRCM_{x1}_XPS_TRCM_{x1} specimen, only after three completed cycles.

Application of a TRM-free thermal insulating (XPS) panel by means of the PVA fiber-reinforced AAM mortar (W_XPS) changed the failure mode from a stepwise-shear observed in the Control specimen to a flexure-governed; Failure occurred in the vicinity of the mid-span (Fig. 7f) at a 30 % and 85 % respectively higher peak load and dissipated energy than in the case of Control specimen. No XPS debonding from the AAM-based mortar was observed during the in-plane tests despite the fact that no mechanical connectors were used (Fig. 7d, f).

For the same amount of fibers employed, single-sided TRAAM-based seismic and combined seismic and energy retrofitting schemes showed higher efficiency (approximately three times) in deformation/energy dissipation terms in respect to the double-sided one. Despite the moderately higher strength gain (20 %) of the double-sided TRAAM retrofitting configuration, the single-sided ones undergo an (energy-consuming) interlaminar shear-driven deterioration prior to failure due to fibers rupture, which affected the overall performance of latter configuration to be more efficient compared to the prior one.

3.2. *Out-of-plane four-point bending tests*

While the Control specimen failed in the vicinity of the midspan

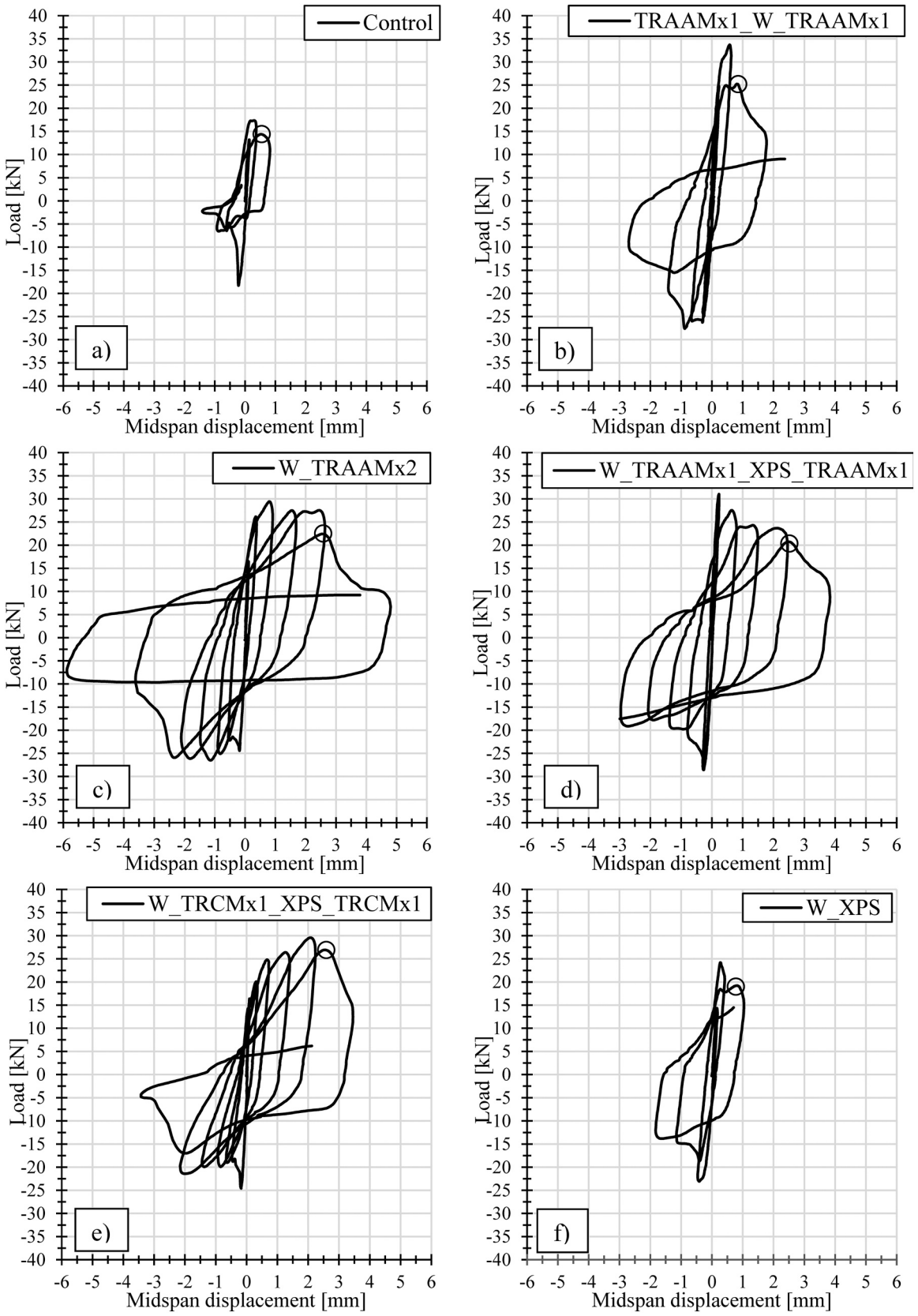

Fig. 8. In-plane testing results for beam-type masonry walls: a) Control; b) $TRAAM_{x1}$_W_$TRAAM_{x1}$; c) W_$TRAAM_{x2}$; d) W_$TRAAM_{x1}$_XPS_$TRAAM_{x1}$; e) W_$TRCM_{x1}$_XPS_$TRCM_{x1}$; f) W_XPS0.

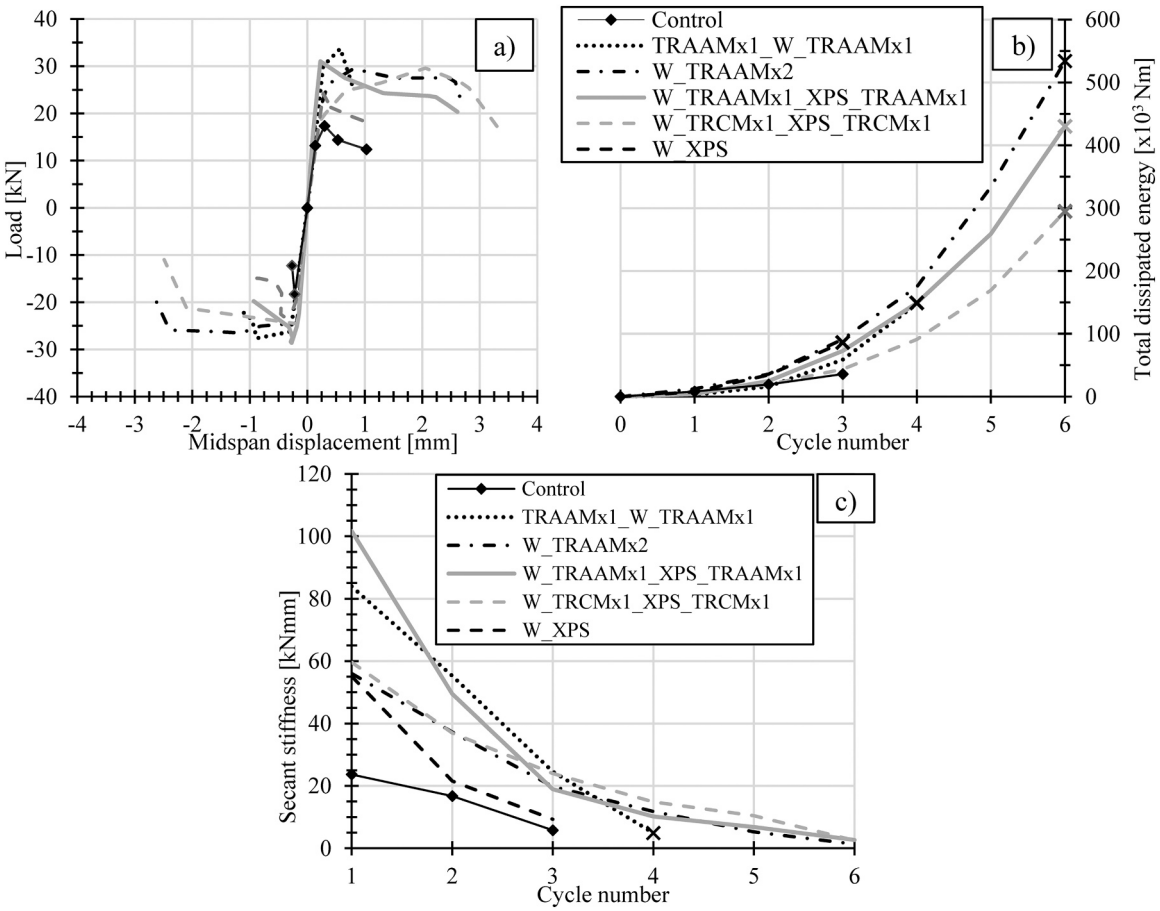

Fig. 9. Comparison of the in-plane testing outcomes for beam-type masonry walls: a) envelopes of the hysteresis diagrams; b) cumulative energy dissipation; c) secant stiffness in each cycle prior to complete failure of the specimen.

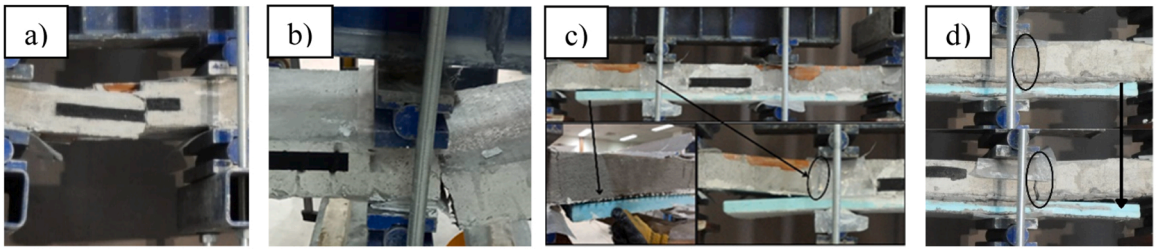

Fig. 10. Out-of-plane test failures: *flexure* - a) Control; *textile rupture* - b) TRAAM$_{x1}$_W_ TRAAM$_{x1}$; *XPS debonding/textile rupture* - c) W_TRCM$_{x1}$_XPS_TRCM$_{x1}$; *Textile rupture/XPS debonding* – d) W_TRAAM$_{x1}$_XPS_TRAAM$_{x1}$.

during the third cycle of the out-of-plane test (Fig. 10a), specimens TRAAM$_{x1}$_W_TRAAM$_{x1}$ and W_TRAAM$_{x2}$ failed at the cross-section of the maximum shear and bending moment near the (right) loading point (Fig. 10b) during the sixth loading cycle. The out-of-plane response of TRAAM-retrofitted walls was heavily affected by the occurrence of glass-fiber rovings' early rupture (Fig. 11b, c), caused by the chemical deterioration of SBR-coated textile, which was confirmed later through a durability study. Consequently, the peak load sustained by TRAAM$_{x1}$_W_TRAAM$_{x1}$ was only 15 % higher than that of the unretrofitted (Control) specimen. Simultaneous activation of two TRAAM layers in the push direction (W_TRAAM$_{x2}$) resulted in a peak load increase of 80 %, while in the pull direction the peak loads were similar to those of the Control specimen (Fig. 11a, c). Despite the higher peak load and ductility of the W_TRAAM$_{x2}$ in the downward direction (Table 5), the total dissipated energy of TRAAM$_{x1}$_W_TRAAM$_{x1}$ was 13 % higher than that of the W_TRAAM$_{x2}$. The unretrofitted upward facing side of the wall caused a highly asymmetric response of the W_TRAAM$_{x2}$ (Fig. 11c).

The behavior of W_TRAAM$_{x1}$_XPS_TRAAM$_{x1}$ was quite similar to the wall retrofitted with two TRAAM layers applied on a single side (W_TRAAM$_{x2}$) (Fig. 11c, d). The first major crack developed in the vicinity of the right loading point in the pull direction, during the second loading cycle. The second major crack was observed near the left loading point zone during the fifth cycle in the pull direction; this was followed by partial debonding of the XPS panel from the left end of the wall. Failure of the inner TRAAM jacket during the seventh cycle was followed by detachment of the XPS panel from the wall's right end, which completely annulled the load-bearing capacity of the specimen (Fig. 10d). The limited load transfer through the XPS middle layer to the outer TRAAM layer was caused by the significantly lower stiffness of the XPS compared to the mortar material. As a result, the 15 % lower peak loads were sustained in the downward direction by the W_TRAAM$_{x1}$_XPS_TRAAM$_{x1}$ despite its higher internal lever arm of the

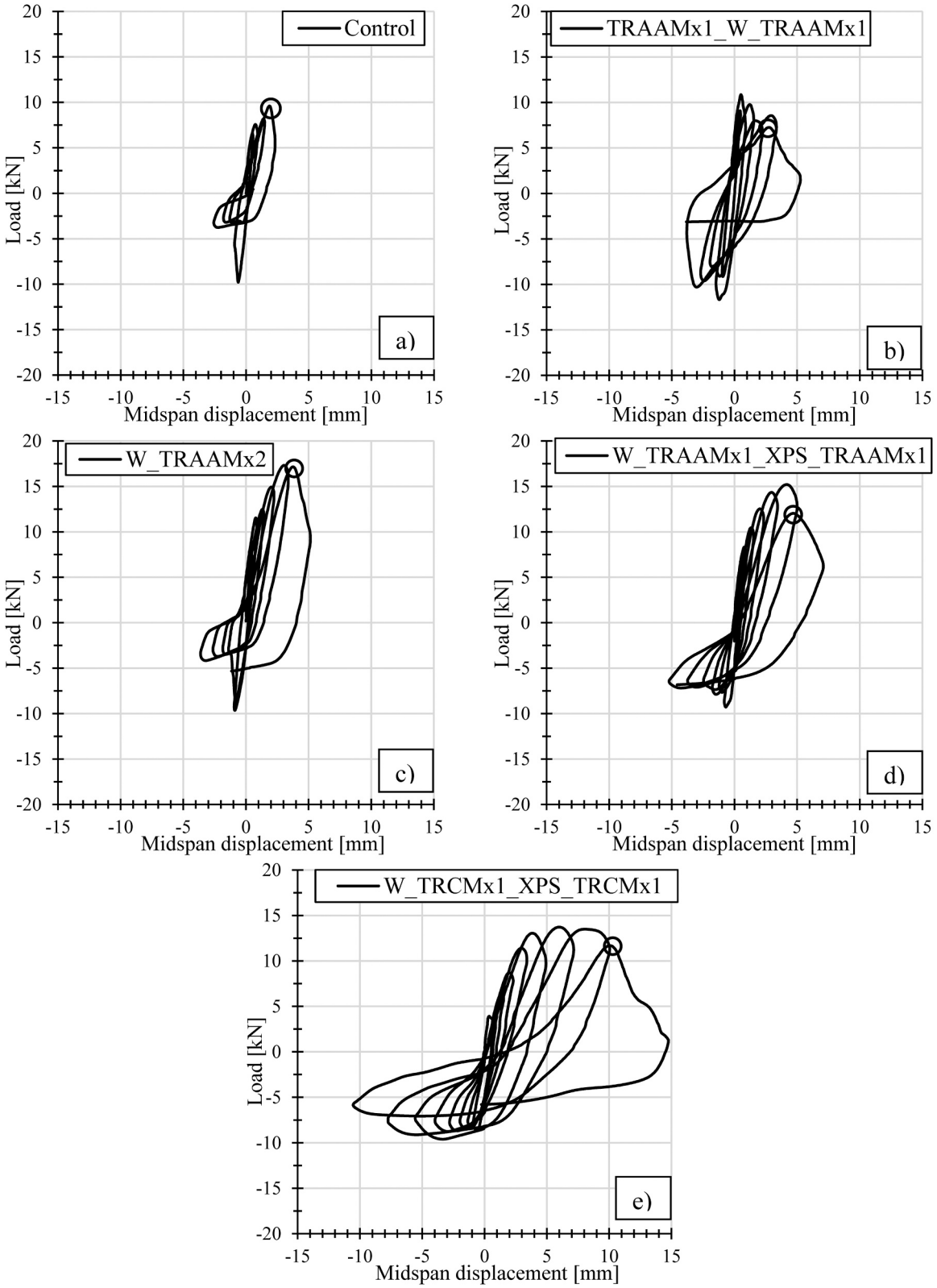

Fig. 11. Out-of-plane testing results for beam-type masonry walls: a) Control; b) $TRAAM_{x1}$_W_TRAAM_{x1}; c) W_TRAAM_{x2}; d) W_TRAAM_{x1}_XPS_TRAAM_{x1}; e) W_TRCM_{x1}_XPS_TRCM_{x1};.

outer TRAAM layer than that of the W_TRAAM_{x2}.

The wall specimen retrofitted with the OPC-based configuration (W_TRCM_{x1}_XPS_TRCM_{x1}) performed significantly better than its AAM-based counterpart. The initial major cracking that occurred at the left loading point during the second cycle was followed by partial debonding of the XPS panel from the left end of the W_TRCM_{x1}_XPS_TRCM_{x1} specimen. Debonding of the XPS, in this case, due to fracture Mode I phenomena was rather inevitable and (as in the in-plane loading case) mortar-dependent. A gradual decrease of stiffness in the push direction can be observed in Fig. 11e, until the extremity of the XPS panel

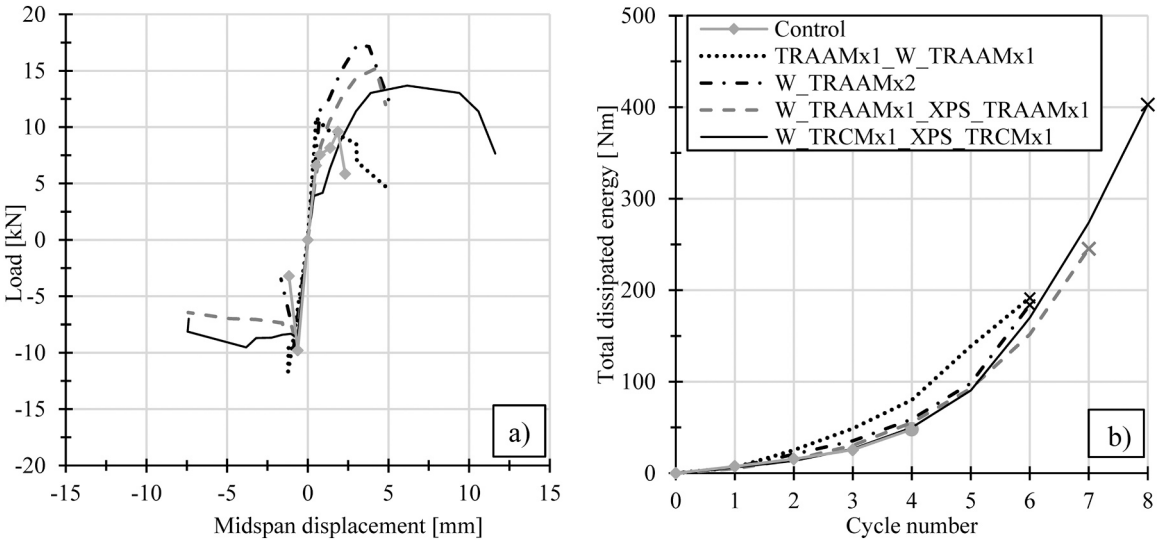

Fig. 12. Comparison of the out-of-plane testing outcomes for beam-type masonry walls: a) envelopes of the hysteresis diagrams; b) cumulative energy dissipation.

detached from the OPC-based mortar, resulting in a short plateau in the seventh cycle (Fig. 11e). Complete failure was initiated by fiber-rovings' rupture of the inner TRCM layer during the eighth loading cycle (Fig. 10d). The combined seismic and energy retrofitting system increased the peak vertical loads by 60 % and 40 % when the TRAAM and TRCM jackets were activated (in tension), respectively. Such a low increase can be attributed to the limited bond characteristics of the XPS panels (especially, in the presence of Mode-I debonding conditions), and to the suspected durability issues of the SBR-coated glass-fiber textile caused by the high alkalinity of the applied alkali-activated mortar (AAM). Application of the combined AAM-based retrofitting configuration (W_TRAAM$_{x1}$_XPS_TRAAM$_{x1}$) increased the energy dissipation and the average deformation capacity (in the push and pull direction) by 380 % and 135 %, respectively, despite the premature rupture of the glass-textile reinforcement. The total dissipated energy prior to complete failure of the specimen and the average deformation capacity (push and pull) of W_TRCM$_{x1}$_XPS_TRCM$_{x1}$ was 11 and 7.5 times higher, respectively, than that of the control specimen; 620 % and 515 % higher than the respective energy dissipation and deformation capacities of the corresponding W_TRAAM$_{x1}$_XPS_TRAAM$_{x1}$ specimen (Fig. 12). The previous comparison clearly shows the importance of textile durability within the strengthening system and its effect on the overall performance that can be expected in real-world applications. While the debonding of thermal insulating panels can be prevented easily by applying the specialized mechanical anchors, the degradation of the textile reinforcement observed in TRAAM must be resolved in order to consider the proposed AAM-based solution as a viable alternative to the existing OPC-based systems. Application of the TRM jackets increased the initial stiffness of the wall specimens (up to 50 %). However, in absolute numbers these increases are marginal due to the geometry and the testing configuration.

4. Durability of the applied AAM-based TRM

Considering the previously shown results of the material characterization tests and the cyclic tests of TRAAM-retrofitted beam-type masonry walls, a further study on the employed SBR-coated electrical (E) glass-fiber textile was necessary to resolve the suspected durability issues of the tested TRAAM retrofitting scheme. The alkali-resistant SBR coating has proven to be efficient in protecting E-glass fibers exposed to the traditional hydrated cementitious binders, that is environments with the pH of 12.5 ± 0.2 [59]. However, it was reported [59] that TRC specimens consisting of SBR-coated E-glass textile sustained significant damage of the coating and strength degradation under accelerated exposure to high alkalinity (pH = 13.8 ± 0.2).

The fibers embedded in alkali-activated mortars are typically exposed to extreme alkalinities (pH = 14) for a short period of time, which drops gradually during the AAM hardening. Therefore, the durability of glass-fiber textile was studied by testing the TRAAM specimens up to 150 days of age. The findings obtained through tensile tests of TRAAM and bare glass-fiber textiles were correlated to those deriving from fiber-matrix interface mapping through scanning electron

Table 6
Summary of flexural and compressive strength of AAM mortar, and tensile strength and ultimate strain of bare textile strips previously exposed to extremely alkaline environment*, and TRAAM coupons at different ages (st. dev. in parenthesis).

	AAM mortar		Bare textile immersed in the activators' solution* and TRAAM		
Age [days]	Mean flexural strength [MPa]	Mean compressive strength [MPa]	Mean tensile strength per unit width of textile [kN/m']	Mean tensile strength referring to the fibers' cross-section [MPa]	Mean tensile strain at fiber rupture [%]
0(control)	-	-	61.58 (0.50)	1184.30 (9.69)	2.58 (0.33)
1*	-	-	25.49 (7.16)	471.97 (119.23)	0.93 (0.25)
2	5.01 (0.27)	33.75 (1.00)	-	-	-
3*	-	-	10.65 (0.82)	204.73 (15.77)	0.42 (0.03)
7	5.90 (0.42)	40.80 (2.28)	30.74 (1.62)	591.15 (31.13)	0.72 (0.20)
14	5.84 (0.17)	38.28 (0.69)	32.66 (2.29)	627.98 (44.00)	0.49 (0.27)
28	6.62 (0.17)	44.12 (0.65)	27.29 (1.40)	524.89 (26.86)	0.19 (0.05)
90	6.03 (0.29)	44.10 (1.52)	26.51 (4.60)	509.86 (88.50)	0.13 (0.02)
150	7.42 (0.25)	49.35 (0.71)	30.53 (7.49)	587.09 (144.01)	0.19 (0.06)

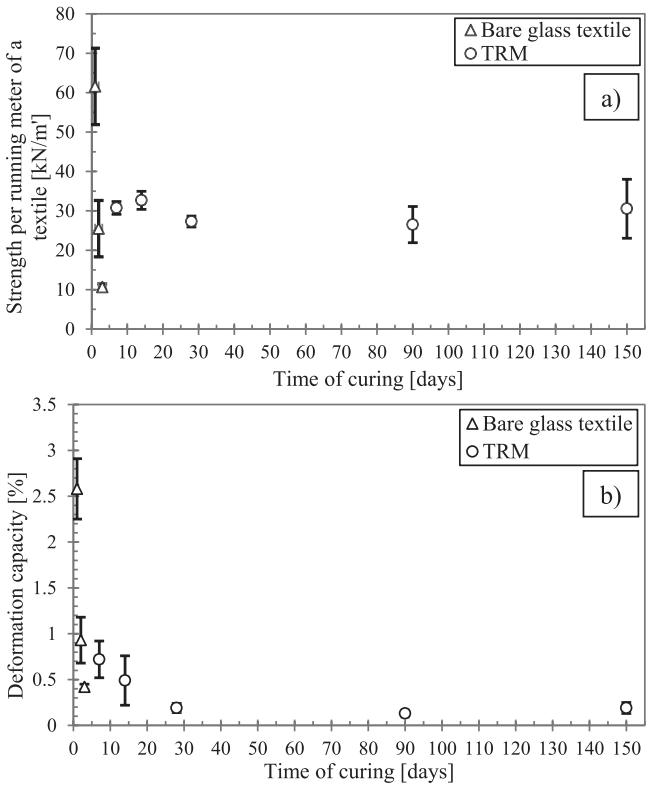

Fig. 13. Tensile strength (a) and deformation capacity development (b) for SBR-coated bare glass-fiber textile and TRAAM coupon specimens.

microscopy (SEM) and energy dispersive X-ray spectroscopy (EDS) analyses.

4.1. Mechanical tests of alkali-activated mortar, TRAAM and bare glass-fiber textile specimens

A minimum of three specimens for each group of TRM coupons were prepared and cured for 7, 14, 28, 90 and 150 days, after which they were tested in uniaxial tension by following the standard testing procedure of AC434 [55]. A total of nine bare SBR-coated glass-fiber textile specimens of the same width (5 rovings in weft direction) with approximate dimensions of 90 mm × 600 mm were also tested according to ISO 13934-1 [56]. Three specimens were not exposed to the alkaline environment and served as control (0 days of exposure), while six were immersed in the activators' solution (Table 1) comprising two separate groups of three specimens each; the first group rested in the solution for 24 h while the second remained in the alkaline bath for 72 h. All textile strips were tested in uniaxial tension after the conclusion of their exposure time periods. The aim of exposing the bare glass-fiber textile specimens directly to the extremely alkaline activating solution (pH = 14, $KOH + K_2SiO_3 + H_2O$) was to study the effect of highly concentrated hydroxides (OH-) on the SBR coating. Specimen preparation, testing setup and procedures applied for the uniaxial tests were identical to the ones applied in the material characterization tests (see Section 2.2). Moreover, the mortar strength development over the 150-day timespan was obtained according to the same procedures applied in the characterization tests (EN196–1) [54] (see Section 2.2).

A summery of the flexural and compressive strength for the employed AAM-based mortar obtained after 2, 7, 14, 28, 90 and 150 days, the tensile strength and deformation capacity of bare textile specimens (control and immersed in the activator's solution for 1 and 3 days) and TRAAM coupons tested at 7, 14, 28, 90 and 150 days of age is shown in Table 6.

An overview of the tensile strength for bare SBR-coated glass-fiber textile and TRAAM as a function of the exposure time to the alkaline environment (activating solution and AAM matrix, respectively) is presented in Fig. 13a, while the deformation capacity (ultimate strain) throughout the studied timespan is shown in Fig. 13b. While the strength and deformation capacity of the bare SBR-coated glass-fiber textile specimens degraded rapidly within a day of exposure, the ultimate tensile strain of the TRAAM decreases more gradually. The tensile strength of TRAAM specimens cured for 7, 14, 28, 90 and 150 days prior to testing remained rather constant.

4.2. Scanning electron microscopy and energy dispersive X-ray spectroscopy analyses

The interface between the AAM matrix and the SBR-coated glass fibers as well as the damage caused by exposure of coating and E-glass fiber materials to the activating solution (pH = 14) was also studied at a microscopic scale. Images were obtained with a "FEI QUANTA FEG 650" equipment with backscattering electrons (BSE) mode and an acceleration of 15 kV under low vacuum conditions at a working distance of 10 mm. Qualitative analysis of localized chemical composition was performed to visualize the potential formation of specific reaction products on the fibers' surface. For the analysis, X-ray energy dispersive spectroscopy (EDS) was used. Preparation of the TRAAM samples involved vacuum impregnation with epoxy resin, water grinding with sandpaper up to 800 μm, and polishing up to 4 μm with a diamond paste. Ultrasonic cleaning was performed after each grinding/polishing step.

SEM image shown in Fig. 14a was taken from the virgin (unexposed) glass-fiber roving sample while the sample immersed in the alkali-activating solution for 3 days is shown in Fig. 14b. The damage of the SBR coating caused by the activators' solution (pH = 14) was observed in the form of white spots and surface microcracks (Fig. 14b), which could allow hydroxyl anions to penetrate through the coating layer and damage the glass fibers by breaking the Si-O bonds of the glass network [60,61]. Clearly, the SBR coating was unable to sustain the short-term

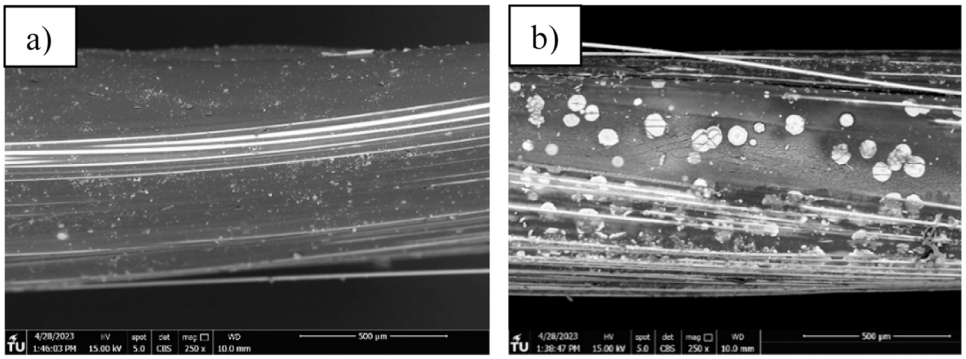

Fig. 14. SEM of SBR-coated glass-fiber roving: a) virgin (unexposed); b) after exposure to activators' solution for 3 days.

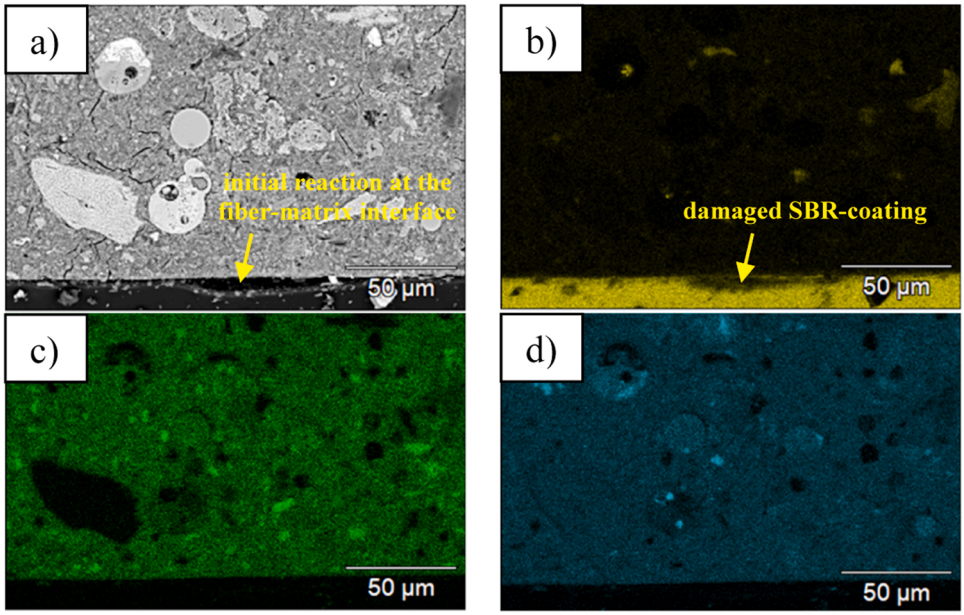

Fig. 15. Element distribution measured by EDS at the interface between the SBR-coated glass-fiber yarn and the AAM matrix (7 days old sample): a) grey image; b) C; c) Al; d) Si.

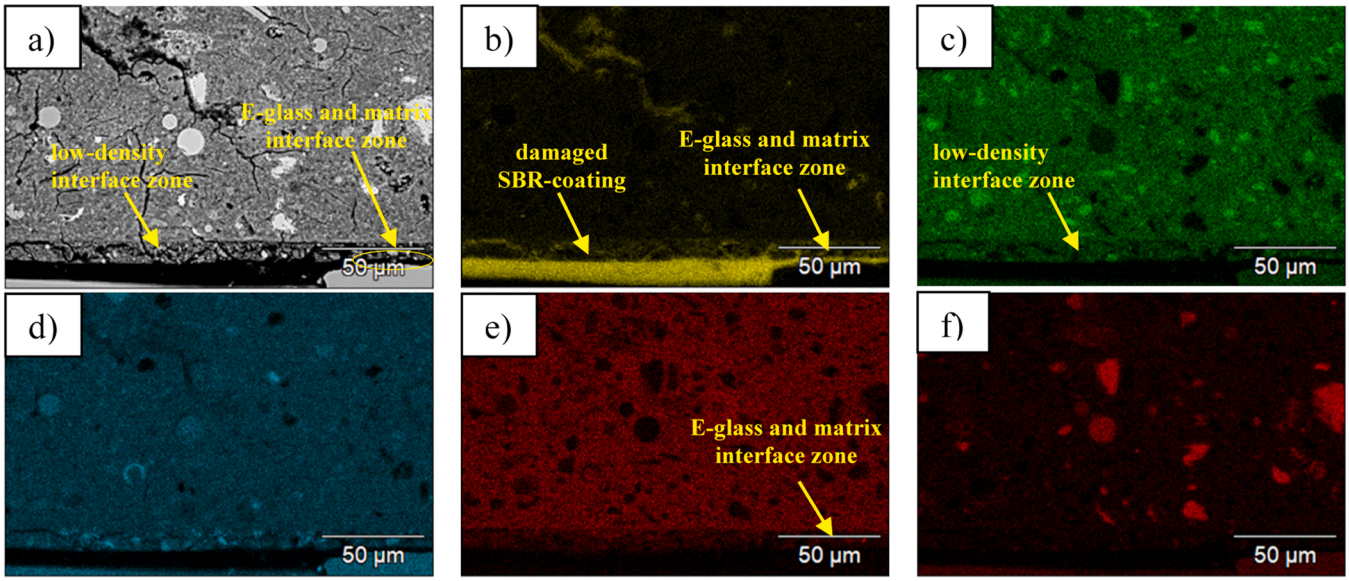

Fig. 16. Element distribution measured by EDS at the interface between the SBR-coated glass-fiber yarn and the AAM mortar (28 days old sample): a) grey image; b) C; c) Al; d) Si; e) K; f) Ca (transition zones are arrow-pointed).

exposure to such a high alkalinity without damage of the inner glass fiber filaments.

Images in Fig. 15 depict the interfacial zone between the AAM matrix and the SBR-coated glass-fiber roving of the 7-day old TRAAM sample. The initial chemical reaction at the fiber-matrix interface is visible in Fig. 15a, and its presence can be confirmed with a lower content of carbon particles (Fig. 15b) at the fiber surface. This indicates a deterioration of the polymeric (SBR) coating.

A low-density gel at the matrix-fiber interface can be observed in the SEM image of the 28-day old TRM samples (Fig. 16a), which clearly confirms the existence of the chemical reaction. Further decay of the SBR coating depicted with the decreasing concentration of carbon is observed in 28-day old samples (Fig. 16b). Some interaction between the outer E-glass filaments and OH^- particles lead to the change of chemical element distribution in the zone of interest (Fig. 16b, e), where carbon is replaced with a low concentration of potassium, which indicates the interaction between the E-glass and the AAM matrix through the damaged coating.

Finally, SEM and EDS analyses of the sample cured for 150 days confirmed the initial findings obtained in 7- and 28-day old TRM samples (Figs. 15, 16). The chemical reactions between the AAM and the SBR-coating can be described as more stable and solid than that of the 28-day old sample (Fig. 17a). The interfacial zone of the 150-day old TRAAM sample which does not contain carbon atoms (Fig. 17b) indicates a complete degradation of the coating in this area; glass fibers are not visible in the sample shown in Fig. 17, which means that the thick SBR coating here prevented their direct exposure. However, a solid network containing aluminum, silicon and potassium (Fig. 17c, d, e) is

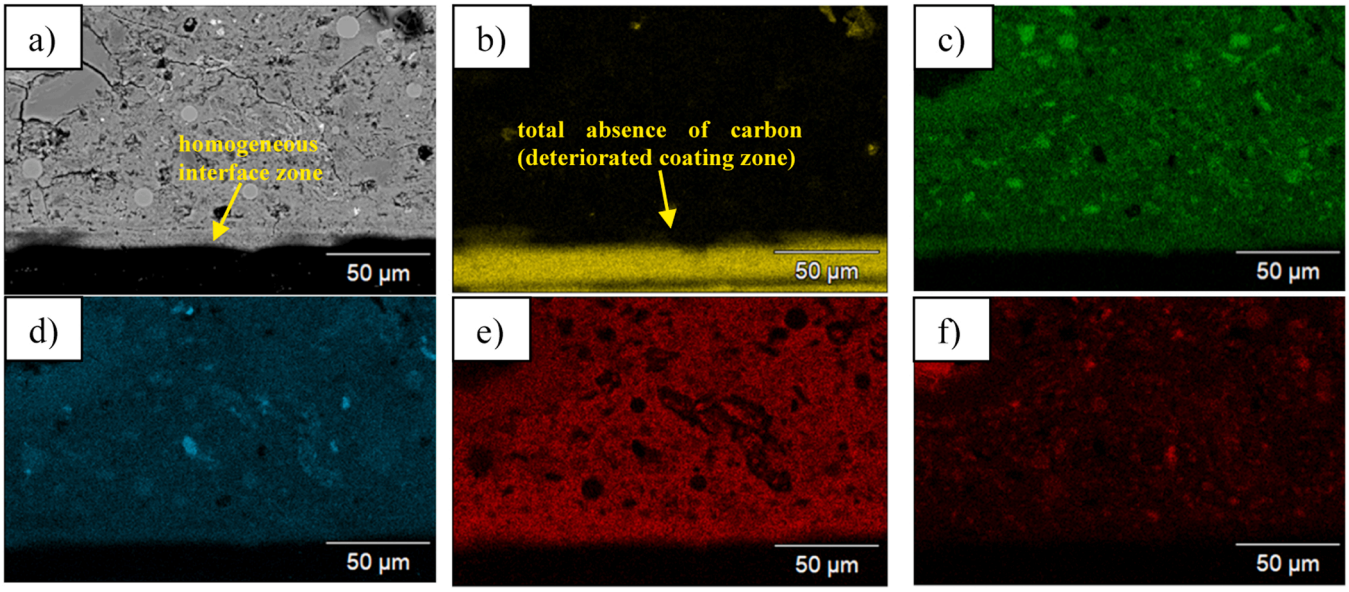

Fig. 17. Element distribution, measured by EDS at the interface between the SBR-coated glass-fiber yarn and the AAM mortar (150 days old sample): a) grey image; b) C; c) Al; d) Si; e) K; f) Ca. (transition zones are arrow-pointed).

clearly visible and it testifies to severe damage of the SBR coating caused by the alkaline environment of the AAM matrix.

The findings of the presented durability study suggest that the alkaline resistance of SBR-coating employed in the employed textile is insufficient to sustain exposure to the extremely alkaline environment caused by the proposed AAM mortar mix design (Table 1), even for a limited time-period. The use of more stable materials that are resistant to high alkalinity, such as carbon or alkali-resistant glass [49,62,63] would significantly improve the durability of the TRAAM strengthening system. Optimization of the coatings' design for high alkalinity exposures [64] could potentially mitigate the durability issues of E-glass textiles. Moreover, by using somewhat less reactive precursor materials, the required concentration of the alkaline activators could potentially decrease, which would reduce the initial alkalinity of the matrix. This way the alkali-resistant coatings (e.g. SBR) designed for traditional cementitious binders could potentially be able to sustain the exposure to AAM mixes designed with lower hydroxyl concentrations. However, extensive research on optimizing the materials for TRAAM strengthening systems is required in order to verify the previous statements.

5. Conclusions

The present study investigates the effectiveness of seismic retrofitting with textile reinforced alkali-activated mortar (TRAAM) and the combined seismic and energy retrofitting (TRAAM and XPS) of beam-type masonry wall models made of single-leaf, perforated fired-clay bricks. For comparison reasons, a configuration comprising a commercial OPC-based TRM and XPS was applied and tested as well (TRCM). Based on the experimental results, the following conclusions can be drawn:

- Seismic, and combined energy and seismic retrofitting of the URM beam-type walls changed the in-plane failure from stepwise, shear-controlled observed in unretrofitted (control) specimen to flexure-controlled. Application of all TRM-based systems on a single side of the wall resulted in: in-plane strength increase of 50 %, small to moderate out-of-plane strength gains, and an increase of in-plane deformation and energy dissipation capacity of approximately 5 and 8 times, respectively.
- Single-sided TRM configurations achieved minor strength increase (10 %) and approximately 3 times higher total energy dissipation during the cyclic in-plane tests compared to the double-sided ones consisting of the same mortar and total amount of textile reinforcement. However, single-sided AAM-based strengthening schemes did not perform very well during the out-of-plane tests. Despite sustaining 50 % higher peak loads than the corresponding double-sided scheme, no benefits of the double-sided AAM-based configurations were observed concerning the out-of-plane deformation and energy dissipation capacity. Moreover, the integrated OPC-based retrofitting system (TRCM/XPS) was at least twice more effective in terms of the sustained deformation during the out-of-plane tests than the AAM-based configurations, while in case of the energy dissipation this margin was even higher.
- Strengthening systems evoking failure due to fibers rupture – that is all TRM-based systems but the TRCM/XPS integrated one – exhibit much less deformation and energy dissipation capacity compared to a system capable of controlled XPS debonding. A potential reason for such an outcome lays in a limited resistance of the SBR-coating to a short-term exposure to very high alkalinity.
- The use of an intermediate XPS layer in one-sided double-layered TRM overlays infers minimal in-plane strength reductions, but bears a toll on both the deformation and the energy dissipation capacity of the strengthened elements subjected to in-plane loading. The poor stress transfer capacity of the XPS layer and its debonding from the mortar (AAM and OPC) which was particularly observed during the out-of-plane cyclic tests, seems to cancel any out-of-plane strength increase effects owing to the increase of the outer TRM layer lever arm. More tests should be carried out for better understanding and characterization of the bond between the extruded polystyrene (XPS) and geopolymer (AAM) mortars.

- Deterioration of TRM made of SBR-coated E-glass-fiber textile and AAM mortar was confirmed through a set of tensile tests carried out on specimens cured over a 150-day timespan. SEM and EDS analyses of the matrix-fiber interface confirmed that the alkali-resistant SBR-coating is susceptible to deterioration under high alkalinity. Direct short-term exposure of bare-textile to the activating solution confirmed that the employed SBR-coating cannot sustain high levels of alkalinity (pH=14) even for extremely short time intervals without a significant damage. To overcome the observed durability issues, further research on the materials optimization (AAM mortar mix design and coatings) is required.

- The use of geopolymers (AAM) as matrix materials in the TRM and TRC composites represents quite a promising concept due to the good adhesive and mechanical properties of AAMs in general, as well as their potential to substantially lower the carbon footprint of both composite systems. Involving these materials in a systematic mechanical and energy upgrading of the existing building stock could be profoundly beneficial. However, durability and reliability of the AAM-based textile reinforced composites must be assured over a planned life cycle period, for these materials to be efficiently used in retrofitting of real-world structures. This study presents an experimental proof of this concept covering some of its benefits and drawbacks. However, a significant amount of research needs to be carried out before reaching the point where AAM-based textile reinforced composites (TRM or TRC) will be massively used in renovation and retrofit of the existing masonry buildings.

CRediT authorship contribution statement

Lazar D. Azdejkovic: Writing – original draft, Visualization, Methodology, Investigation, Conceptualization. **Thanasis C. Triantafillou:** Writing – review & editing, Validation, Supervision, Project administration, Conceptualization. **Catherine G. Papanicolaou:** Writing – review & editing, Validation. **Luiz Miranda de Lima:** Methodology, Investigation.

Declaration of Competing Interest

The authors declare that they have no known competing financial interests or personal relationships that could have appeared to influence the work reported in this paper.

Acknowledgements

This research has received funding from the European Union's Horizon 2020 research and innovation programme under grant agreement No 813596 DuRSAAM. The contents of this publication are the sole responsibility of the author and do not necessarily reflect the opinion of the European Union.

Data availability

Data will be made available on request.

References

[1] Economidou M, Todeschi V, Bertoldi P, D'Agostino D, Zangheri P, Castellazzi L. Review of 50 years of EU energy efficiency policies for buildings. Energy Build 2020;225:110322. https://doi.org/10.1016/j.enbuild.2020.110322.
[2] Curbach M, Jesse F. High-performance textile-reinforced concrete. Struct Eng Int 1999;9(4):289–91.
[3] Triantafillou TC, Papanicolaou CG, Zissimopoulos P, Laourdekis T. Concrete confinement with textile-reinforced mortar jackets. Acids Struct J 2006;103(1):28–37. https://doi.org/10.14359/15083.
[4] Papanicolaou CG, Triantafillou TC, Karlos K, Papathanasiou M. Textile-reinforced mortar (TRM) versus FRP as strengthening material of URM walls: in-plane cyclic loading. Mater Struct 2007;40(10):1081–97. https://doi.org/10.1617/s11527-006-9207-8.
[5] Papanicolaou CG, Triantafillou TC, Papathanasiou M, Karlos K. Textile reinforced mortar (TRM) versus FRP as strengthening material of URM walls: Out-of-plane cyclic loading. Mater Struct 2008;41(1):143–57. https://doi.org/10.1617/s11527-007-9226-0.
[6] Augenti N, Parisi F, Prota A, Manfredi G. In-plane lateral response of a full-scale masonry subassemblage with and without an inorganic matrix-grid strengthening system. J Compos Constr 2011;15(4):578–90. https://doi.org/10.1061/(ASCE)CC.1943-5614.0000193.
[7] Ismail N, Ingham JM. In-plane and out-of-plane testing of unreinforced masonry walls strengthened using polymer textile reinforced mortar. Eng Struct 2016;118:167–77. https://doi.org/10.1016/j.engstruct.2016.03.041.
[8] Gattesco N, Boem I, Rizzi E, Dudine A, Gams M. Cyclic tests on two-leaf rubble stone masonry spandrels strengthened with CRM coating on one or both sides. Eng Struct 2023;296:116965. https://doi.org/10.1016/j.engstruct.2023.116965.
[9] Bertolesi E, Buitrago M, Giordano E, Calderón PA, Moragues JJ, Clementi F, et al. Effectiveness of textile reinforced mortar (TRM) materials in preventing seismic-induced damage in a U-shaped masonry structure submitted to pseudo-dynamic excitations. Constr Build Mater 2020;248:118532. https://doi.org/10.1016/j.conbuildmat.2020.118532.
[10] Giordano E, Bertolesi E, Clementi F, Buitrago M, Adam JM, Ivorra S. Unreinforced and TRM-reinforced masonry building subjected to pseudodynamic excitations: numerical and experimental insights. J Eng Mech 2021;147(12):04021107. https://doi.org/10.1061/(ASCE)EM.1943-7889.0002017.
[11] Harajli M, ElKhatib H, San-Jose JT. Static and cyclic out-of-plane response of masonry walls strengthened using textile-mortar system. J Mater Civ Eng 2010;22(11):1171–80. https://doi.org/10.1061/(ASCE)MT.1943-5533.000012.
[12] Babaeidarabad S, Caso FD, Nanni A. Out-of-plane behavior of URM walls strengthened with fabric-reinforced cementitious matrix composite. J Compos Constr 2014;18(4):04013057. https://doi.org/10.1061/(ASCE)CC.1943-5614.000045.
[13] Krevaikas TD. Experimental study on carbon fiber textile reinforced mortar system as a means for confinement of masonry columns. Constr Build Mater 2019;208:723–33. https://doi.org/10.1016/j.conbuildmat.2019.03.033.
[14] Koutas LN, Bournas DA. Confinement of masonry columns with textile-reinforced mortar jackets. Constr Build Mater 2020;258:120343. https://doi.org/10.1016/j.conbuildmat.2020.120343.
[15] Fetting C. "The European Green Deal", ESDN report, December 2020, ESDN Office, Vienna; 2020.
[16] Dalalbashi A, Ghiassi B, Oliveira DV. Textile-to-mortar bond behaviour in lime-based textile reinforced mortars. Constr Build Mater 2019;227:116682. https://doi.org/10.1016/j.conbuildmat.2019.116682.
[17] Tamburini S, Natali M, Garbin E, Panizza M, Favaro M, Valluzzi MR. Geopolymer matrix for fibre reinforced composites aimed at strengthening masonry structures. Constr Build Mater 2017;141:542–52. https://doi.org/10.1016/j.conbuildmat.2017.03.017.
[18] Cholostiakow S, Koutas LN, Papakonstantinou CG. Geopolymer versus cement-based textile-reinforced mortar: diagonal compression tests on masonry walls representative of infills in RC frames. Constr Build Mater 2023;373:130836. https://doi.org/10.1016/j.conbuildmat.2023.130836.
[19] Donnini J, Mobili A, Maracchini G, Chiappini G, Tittarelli F, Corinaldesi V. A multi-performance comparison between lime, cementitious and alkali-activated TRM systems: mechanical, environmental and energy perspectives. Constr Build Mater 2024;440:137396. https://doi.org/10.1016/j.conbuildmat.2024.137396.
[20] Pepe M, Lombardi R, Ferrara G, Agnetti S, Martinelli E. Experimental characterisation of lime-based textile-reinforced mortar systems made of either jute or flax fabrics. Materials 2023;16(2):709.
[21] Gkournelos PD, Azdejković LD, Triantafillou TC. Innovative and eco-friendly solutions for the seismic retrofitting of natural stone masonry walls with textile reinforced mortar: in-and out-of-plane behavior. J Compos Constr 2022;26(1):04021061. https://doi.org/10.1061/(ASCE)CC.1943-5614.0001173.
[22] Torres B, Ivorra S, Baeza FJ, Estevan L, Varona B. Textile reinforced mortars (TRM) for repairing and retrofitting masonry walls subjected to in-plane cyclic loads. An experimental approach. Eng Struct 2021;231:111742. https://doi.org/10.1016/j.engstruct.2020.111742.
[23] Elghazouli AY, Bompa DV, Mourad SA, Elyamani A. In-plane lateral cyclic behaviour of lime-mortar and clay-brick masonry walls in dry and wet conditions. Bull Earthq Eng 2021;19:5525–63. https://doi.org/10.1007/s10518-021-01170-5.
[24] Davidovits J. Geopolymers: inorganic polymeric new materials. J Therm Anal Calorim 1991;37(8):1633–56.
[25] Provis JL. Geopolymers and other alkali activated materials: why, how, and what? Mater Struct 2014;47:11–25. https://doi.org/10.1617/s11527-013-0211-5.
[26] Krivenko P. Why alkaline activation–60 years of the theory and practice of alkali-activated materials. J Ceram Sci Technol 2017;8(3):323–33.
[27] Carabba L, Santandrea M, Carloni C, Manzi S, Bignozzi MC. Steel fiber reinforced geopolymer matrix (S-FRGM) composites applied to reinforced concrete structures for strengthening applications: a preliminary study. Compos Part B Eng 2017;128:83–90. https://doi.org/10.1016/j.compositesb.2017.07.007.
[28] Zhang HY, Yan J, Kodur V, Cao L. Mechanical behavior of concrete beams shear strengthened with textile reinforced geopolymer mortar. Eng Struct 2019;196:109348. https://doi.org/10.1016/j.engstruct.2019.109348.
[29] Candamano S, Crea F, Iorfida A. Mechanical characterization of basalt fabric reinforced alkali-activated matrix composite: a preliminary investigation. Appl Sci 2020;10(8):2865. https://doi.org/10.3390/app10082865.
[30] Skyrianou I, Papakonstantinou CG, Koutas LN. Investigation of the bond behaviour between geopolymer TRM and concrete. In: RILEM spring convention and conference. Cham: Springer Nature Switzerland; 2024. p. 3–11.
[31] Azdejkovic LD, Triantafillou TC. Seismic retrofit of RC short columns with textile-reinforced alkali-activated or cement-based mortars. J Compos Constr 2023;27(5):04023041. https://doi.org/10.1061/JCCOF2.CCENG-4193.
[32] Arce A, Kapsalis P, Papanicolaou CG, Triantafillou TC. Diagonal compression tests on unfired and fired masonry wallettes retrofitted with textile-reinforced alkali-activated Mortar. J Compos Sci 2023;8(1):14.
[33] Libre Jr RGD, Leaño Jr JL, Lopez LF, Cacanando CJD, Promentilla MAB, Guades EJ, et al. In-plane shear behavior of unreinforced masonry wall strengthened with bamboo fiber textile-reinforced geopolymer mortar. Buildings 2023;13(2):538. https://doi.org/10.3390/buildings13020538.
[34] Longo F, Cascardi A, Lassandro P, Aiello MA. Energy and seismic drawbacks of masonry: a unified retrofitting solution. J Build Pathol Rehabil 2021;6:1–24.
[35] Marini A, Passoni C, Riva P, Negro P, Romano E, Taucer F. Technology options for earthquake resistant, eco-efficient buildings in Europe: research needs. European

Commission, Joint Research Centre Scientific and Policy Reports; 2014. https://doi.org/10.2788/68902.
[36] Pohoryles DA, et al. Energy performance of existing residential buildings in Europe: a novel approach combining energy with seismic retrofitting. Energy Build 2020;223:110024. https://doi.org/10.1016/j.enbuild.2020.110024.
[37] Triantafillou TC, Karlos K, Kefalou K, Argyropoulou E. An innovative structural and energy retrofitting system for URM walls using textile reinforced mortars combined with thermal insulation: mechanical and fire behavior. Constr Build Mater 2017; 133:1–13. https://doi.org/10.1016/j.conbuildmat.2016.12.032.
[38] Triantafillou TC, Karlos K, Kapsalis P, Georgiou L. Innovative structural and energy retrofitting system for masonry walls using textile reinforced mortars combined with thermal insulation: In-plane mechanical behavior. J Compos Constr 2018;22 (5):04018029. https://doi.org/10.1061/(ASCE)CC.1943-5614.0000869.
[39] Gkournelos PD, Bournas DA, Triantafillou TC. Combined seismic and energy upgrading of existing reinforced concrete buildings using TRM jacketing and thermal insulation. Earthq Struct 2019;16(5):625–39. https://doi.org/10.12989/eas.2019.16.5.625.
[40] Gkournelos PD, Triantafillou TC, Bournas DA. Integrated structural and energy retrofitting of masonry walls: effect of in-plane damage on the out-of-plane response. J Compos Constr 2020;24(5):04020049. https://doi.org/10.1061/(ASCE)CC.1943-5614.0001066.
[41] Karlos K, Tsantilis A, Triantafillou T. Integrated seismic and energy retrofitting system for masonry walls using textile-reinforced mortars combined with thermal insulation: experimental, analytical, and numerical study. J Compos Sci 2020;4(4): 189. https://doi.org/10.3390/jcs4040189.
[42] Gkournelos PD, Triantafillou TC. Out-of-plane behavior of in-plane damaged masonry infills retrofitted with TRM and thermal insulation. J Compos Constr 2023;27(6):04023054. https://doi.org/10.1061/JCCOF2.CCENG-432.
[43] Habert G, Ouellet-Plamondon C. Recent update on the environmental impact of geopolymers. RILEM Tech Lett 2016;1:17. https://doi.org/10.21809/rilemtechlett.2016.6.
[44] Shehata N, Sayed ET, Abdelkareem MA. Recent progress in environmentally friendly geopolymers: a review. Sci Total Environ 2021;762:143166. https://doi.org/10.1016/j.scitotenv.2020.143166.
[45] Salas DA, Ramirez AD, Ulloa N, Baykara H, Boero AJ. Life cycle assessment of geopolymer concrete. Constr Build Mater 2018;190:170–7. https://doi.org/10.1016/j.conbuildmat.2018.09.123.
[46] Giordano E, Masciotta MG, Clementi F, Ghiassi B. Numerical prediction of the mechanical behavior of TRM composites and TRM-strengthened masonry panels. Constr Build Mater 2023;397:132376. https://doi.org/10.1016/j.conbuildmat.2023.132376.
[47] Murgo FS, Ferretti F, Mazzotti C. A discrete-cracking numerical model for the in-plane behavior of FRCM strengthened masonry panels. Bull Earthq Eng 2021;19 (11):4471–502. https://doi.org/10.1007/s10518-021-01129-6.
[48] Wang X, Ghiassi B, Oliveira DV, Lam CC. Modelling the nonlinear behaviour of masonry walls strengthened with textile reinforced mortars. Eng Struct 2017;134: 11–24. https://doi.org/10.1016/j.engstruct.2016.12.029.
[49] Alexander AE, Shashikala AP. Studies on the mechanical and durability performance of textile reinforced geopolymer concrete beams. Mater Today Commun 2023;35:105837. https://doi.org/10.1016/j.mtcomm.2023.105837.
[50] Le Chi H, Louda P, Le Van S, Volesky L, Kovacic V, Bakalova T. Composite performance evaluation of basalt textile-reinforced geopolymer mortar. Fibers 2019;7(7):63. https://doi.org/10.3390/fib7070063.
[51] Trindade ACC, Silva FA, Alcamand HA, Borges PHR. On the durability behavior of natural fiber reinforced geopolymers. In: Proceedings of the 41st international conference on advanced ceramics and composites: ceramic engineering and science proceedings, 38(3). Hoboken, NJ, USA: John Wiley & Sons, Inc; 2018. p. 215–28. https://doi.org/10.1002/9781119474746.ch20.
[52] Farhan KZ, Johari MAM, Demirboğa R. Impact of fiber reinforcements on properties of geopolymer composites: a review. J Build Eng 2021;44:102628. https://doi.org/10.1016/j.jobe.2021.102628.
[53] Azdejkovic L. Seismic retrofitting with alkali-activated textile reinforced mortar (AAM-TRM) (Ph.D. thesis). University of Patras; 2024. ⟨https://hdl.handle.net/10889/27013⟩.
[54] EN 196-1. Methods of testing cement - part 1: determination of strength. European Committee for Standardization; 2016.
[55] AC434. Acceptance criteria for masonry and concrete strengthening using fiber-reinforced cementitious matrix (FRCM) composite systems. A subsidiary of the International Code Council; 2011.
[56] ISO 13934-1 (International Organization for Standardization). Textiles - tensile properties of fabrics part 1: determination of maximum force and elongation at maximum force using the strip method; 2013.
[57] Beyer K. Peak and residual strengths of brick masonry spandrels. Eng Struct 2012; 41:533–47. https://doi.org/10.1016/j.engstruct.2012.03.015.
[58] FEMA461 (Federal Emergency Management Agency). Interim testing protocols for determining the seismic performance characteristics of structural and nonstructural components; 2007.
[59] Paul S, Gettu R, Arnepalli DN, Samanthula R. Experimental evaluation of the durability of glass textile-reinforced concrete. Constr Build Mater 2023;406: 133390. https://doi.org/10.1016/j.conbuildmat.2023.133390.
[60] Chu W, Wu L, Karbhari VM. Durability evaluation of moderate temperature cured E-glass/vinylester systems. Compos Struct 2004;66(1-4):367–76. https://doi.org/10.1016/j.compstruct.2004.04.058.
[61] Bashir ST, Yang L, Liggat JJ, Thomason JL. Kinetics of dissolution of glass fibre in hot alkaline solution. J Mater Sci 2018;53:1710–22. https://doi.org/10.1007/s10853-017-1627-z.
[62] Cousin P, Hassan M, Vijay P, Robert M, Benmokrane B. Chemical resistance of carbon, basalt, and glass fibers used in FRP reinforcing bars. J Compos Mater 2019; 53(26-27):3651–70. https://doi.org/10.1177/0021998319844306.
[63] Shafei B, Kazemian M, Dopko M, Najimi M. State-of-the-art review of capabilities and limitations of polymer and glass fibers used for fiber-reinforced concrete. Materials 2021;14(2):409. https://doi.org/10.3390/ma140204099.
[64] Mader E, Plonka R, Schiekel M, Hempel R. Coatings on alkali-resistant glass fibres for the improvement of concrete. J Ind Text 2004;33(3):191–207. https://doi.org/10.1177/1528083704039833.